1998 Second International Conference on Knowledge-Based Intelligent Electronic Systems, 21-23 April 1998, Adelaide, Australia. Editors, L.C. Jain and R.K.Jain

Implementation of a Pearl Visual Simulator Based on Blurring and Interference

Toshimasa Dobashi†
Noriko Nagata††
Yoshitsugu Manabe†
Seiji Inokuchi†

†Graduate School of Engineering Science
Osaka University
Toyonaka, 560 Japan
dobashi@inolab.sys.es.osaka-u.ac.jp

††Industrial Electronics & Systems Laboratory
Mitsubishi Electric Corporation
Amagasaki, 661 Japan
nagata@con.sdl.melco.co.jp

Keywords: Computer Graphics, Pearl, Physics-Based Modeling, Blurring, Multilayer Thin-film Interference, Monte Carlo

Abstract

Visual simulation using computer graphics has attracted wide attention in many fields. In this paper, we propose a method of modeling and visualizing pearls to implement a pearl visual simulator. Pearls manifest a very specific optical phenomenon. To investigate this feature, we propose a physical model of blurring and pearl interference. The experimental results show that the physics-based-modeling of internal blurring in the multi-layer of a pearl and the partial coherent interference model are effective for high quality pearl visualization. This paper finally describes the possibility that this simulator can be practically used in jewelry shops.

1. Introduction

There have been many studies in various fields to add sensitive values such as "uniqueness" and "delicacy" to the conventional computer graphics representations [1,2]. The authors began research using machine vision technology in 1992 [3,4] for the evaluation of pearl quality requiring intuitive expertise even during inspection in the production process. Later, the visual simulation technique was introduced, and a visual simulator was experimentally produced to investigate the optimization of inspection conditions and normalization of standards [5]. The purpose was to carry out modeling of the optical behavior conforming as closely as possible to the physical model (physics-based-modeling) in order to clarify how the physical parameters contribute to the pearl quality. This approach uses a process of condifying the expertise of the specialists in this field, and can be ranked as an 'analysis-by-synthesis' method in the field of pattern recognition.

Pearls, widely known as a jewelry items, have a multilayer thin-film structure, and display a unique rainbow color and a lustrous iridescence due to the diverse behavior of light such as refraction, interference, diffraction, multiple reflection, etc. [6]. The modeling and visualization of a pearl with specific optical and structural features is an interesting theme. The study of the optical phenomenon of pearl mica paint has previously been reported [7], however no research has yet been made on the optical phenomenon of actual pearls. The authors succeeded in a previous work [5] in achieving a realistic representation of a pearl ('peal-like quality') by means of three principal factors, the interference component, mirroring component and texture component by

0-7803-4316-6/98/$10.00 ©1998 IEEE

using physics-based-modeling.

This paper indicates the importance of the blurring of light, as a fourth factor, to improve the representation of delicate appearance, and proposes the physical model and algorithm.

The blurring of light in a translucent body is caused by the internal spread of light, which is normally explained by the scattering of light. Research into the simulation of the scattering phenomenon has often been reported [8-10]. However, the blur observed in a pearl is considered a phenomenon different from the mere scattering of light. In this paper, the authors explain the blur in a pearl as the spread of light caused by repeated specular reflection and transmission, and produce the blurring component image through simulation.

Further, a new model is also proposed, including coherent light in addition to the incoherent light so far considered in the visualization of interference phenomenon. The paper finally describes a pearl visual simulator equipped with the aforesaid functions, indicating that the newly developed system can be effectively used in a jewelry shop.

2. Physical model of a pearl

This section deals with the previously announced model [5] of multilayer thin-film interference of a pearl and the pearl image synthesis algorithm required to explain the interference and blurring models proposed in this paper.

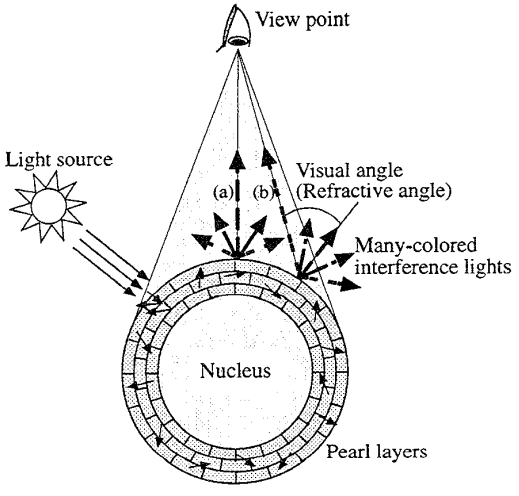

Fig. 1. A physical model of multilayer thin-films of a pearl.

2.1 Physical model of multilayer thin-films interference

Pearls show a very specific optical phenomenon that is not seen in the normal thin-film interference. The color fringe changes concentrically from the center of the sphere, and also can be observed even on the part where light does not hit directly. In other words, the interference color of a pearl depends solely on the viewing direction, and not on the direction of the light source.

The physical model of multilayer thin-films of a pearl shown in Fig. 1 can be used to explain this phenomenon. The incident light is distributed to the whole pearl layer through repeated reflection and refraction. As a result, it appears as if each point in the layer had a point light source transmitting rays in all directions (called an "illuminant model"). Each ray causes local interference and interference lights are propagated in all directions outside the pearl. Taking account of only the interference light waves propagated in the viewing direction *a* and *b* in Fig. 1, the light from each point on the concentric circle is the interference light propagated with the same angle of refraction, so that the phase difference, i.e. the spectrum distribution must be equivalent. This accounts for the fact that the hue of the interference light does not depend on the direction of light source and shows concentric circular change.

2.2 Calculation algorithm of interference light spectrum

The power spectrum of interference light is calculated in the following manner. First, rays are cast from the viewpoint, and for all rays intersecting rays with the pearl surface, the incident angle, reflectance and transmittance are calculated. Next, interference calculations are made from the outer layer to the inner layer of the nacreous layer for all visible wavelength bands in order to obtain the spectral power. By converting the spectrum obtained into an RGB image, an interference light component, which we will describe in the next sub-section, is generated.

2.3 Synthesis of a pearl image

The synthesis algorithm is based on three psychological factors, the sense of depth, brightness and grain, used previously by the authors in their psychological experiments to evaluate the pearl [4]. In other words, the interference component, mirroring component and

texture component, corresponding to the psychological factors, are synthesized on the diffuse reflection component image. The components and a synthesized image are shown in Fig. 2.

Using these methods a pearl has been successfully represented. However, some experts pointed out the lack of the sense of brightness in the synthesized images. The sense of brightness of a pearl is a material feeling deeply related with not only the intensity of specular light but the sense of transparency and of gloss. In the next section, the representation of the sense of brightness is explained.

3. Simulation of blurring

Pearl representation has so far been carried out mainly through interference simulation, so the representation of other factors were not fully considered because of the adoption of conventional shading models.

Most general shading models uses only the information of the object surface, and cannot represent the uniqueness coming from the subsurface structure.

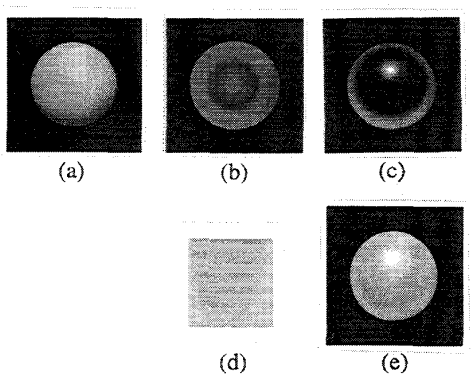

(a) Diffuse component (b) Interference component
(c) Mirroring component (d) Texture component (value)
(e) Synthesized image

Fig. 2. Components and a synthesized image. (Original: Color)

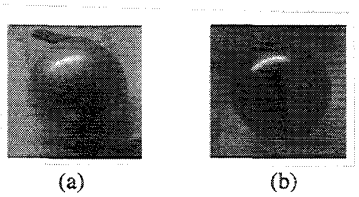

Fig. 3. Blurring of light.

This section proposes the model of blurring and the synthesis algorithm to represent a sense of brightness.

3.1 Blurring model of pearl due to subsurface reflection

The blurring of light in a translucent body is normally explained by the scattering phenomenon. The various types of scattering include isotropic scattering where the light scatters uniformly in all directions, Rayleigh scattering and Mie scattering caused by fine particles in atmosphere.

However, the blurring of light in a pearl is quite different from these. Figure 3 shows an example of the blurring of light seen in a pearl. Figure 3a shows an reflection pattern of a fluorescent light on a pearl, and Fig. 3b shows the reflection pattern on a gold coated pearl. The surface of the pearl is coated with gold 10-30μm thick to prevent light from entering the subsurface, retaining the surface state.

Because the reflectance of an object varies according to its refractive index, the two images can not be directly compared, but it is apparent that appearance of the reflections of the light source are different in Figs. 3a and 3b. In Fig. 3b a sharp reflection of the light source, a characteristic of a mirror surface, is seen while in Fig. 3a the sharp reflection of light source seen in Fig. 3b together with blurred light around the light image is observed. The luminance of this blurring is stronger around the hi-light than at the point where the light enters nacreous layers at right angles to the surface, indicating that the behavior of the light entering the nacreous surface has the characteristic of direct reflection instead of scattering. The subsurface of a pearl has a layered structure, so specular reflection with strong directivity must be taking place inside the layers as well as on the surface. (Since the photographs have been excessively exposed to light in order to clarify the blurring, the light source image has become saturated, appearing wider than the actual image.)

From these observations of a pearl, the blurring in a pearl can be explained as follows. The quite high transmittance of the nacreous layer causes the light to be repeated reflected and transmitted inside the layer. As a result, the spread of light inside the layer tends to have the property of reflection and transmission rather than scattering. The blurring of light in the nacreous layer is

attributed to the spread of light due to the deviation of light from the direction of the direct reflection.

Proposed below are two algorithms to represent the blurring of light caused by subsurface reflection.

3.2 Simulation using Monte Carlo method

The first algorithm uses the Monte Carlo method which is also applied to the calculation of light scattering. The stochastic process of tracing the reflection and transmission is repeated for the light entering the nacreous layer with a certain incident angle, and the intensity of the light finally leaving the surface is integrated for each outgoing direction to obtain the whole reflection distribution for a certain incident angle.The same process is carried out for each incident direction to calculate the BRDF (bi-directional reflectance distribution function), i. e. the reflectance distribution function with the incident direction and reflection direction as variables. We describe the BRDF in the form of a look-up table.

The calculation procedure is illustrated in Fig. 4. First, it is supposed that a light ray enters the layer with the incident angle, $(\theta_{in}, 0)$, and is reflected or transmitted by a micro-facet with normal vector H and with a slope, $(\theta_{norm}, \phi_{norm})$ against the normal vector N of the layer. The slope of the micro-facet is stochastically determined in the following manner by using the micro-facet distribution function

$$\theta_{norm} = f(R_1) \quad \cdots\cdots (1)$$

$$\phi_{norm} = 2\pi R_2 \quad \cdots\cdots (2)$$

Here, R_1 and R_2 are uniform random numbers, and function f is the probability density function of the normal distribution.

Whether to trace the reflection or the transmission of light is determined stochastically. The incident angle is obtained from the normal direction of the micro-facet, and the reflection/ transmission direction is calculated by using Snell's law. The light energy after the reflection/ transmission is obtained by multiplying the current energy with the reflectance/transmittance calculated by using Fresnel's formula.

The process of tracing the light is repeated until the ray exits the nacreous layer or the intensity of the light falls below the threshold value.

Through repetition of the process of adding the intensity of the light to the solid angle containing the exit direction $(\theta_{out}, \phi_{out})$ we can obtain the reflection distribution for a certain incident angle. By carrying out the same process for all incident angles, we can obtain the BRDF.

Figure 5 shows the BRDF for an incident angle of 30° using the aforesaid method. The BRDF shows non-symmetrical distribution of light with the direction of direct reflection as the center, indicating that the blurring phenomenon is properly simulated.

This algorithm features high-quality simulation. It has the drawback, however, of calling for the preparation of a look-up table beforehand, and fails to satisfy the reliability and continuity unless a large number of experiments are carried out.

3.3 Fast simulation based on reflection distribution

The next algorithm we'd like to propose is more simplified and faster than the previously mentioned model.

The simulation results of the previous model show that the rate of deviation of a ray from the direction of direct reflection/transmission becomes higher as the ray goes through a layer repeating reflections and transmissions.

Assuming that the ray inside the nacreous layer keeps its directivity near the surface, and that the

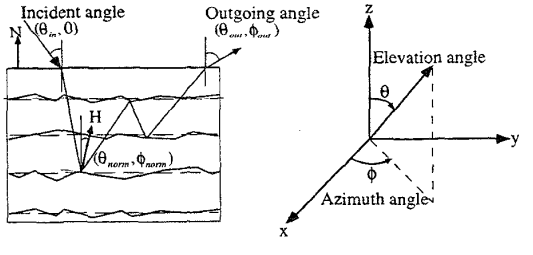

Fig. 4. Simulation using Monte-Carlo algorithm.

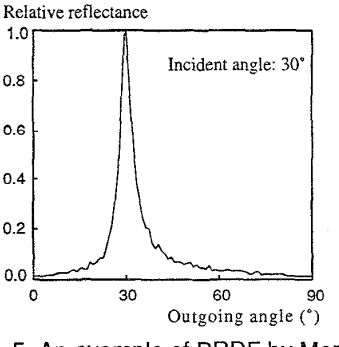

Fig. 5. An example of BRDF by Monte Carlo algorithm

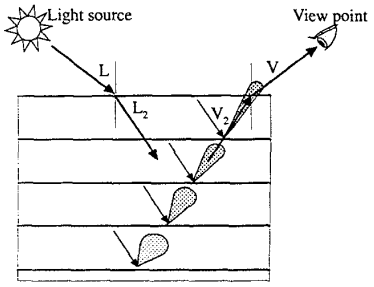

Fig. 6. Fast simulation using specular reflection distribution.

reflection distribution in deeper layers has a wider directivity, and by summing up the reflection distributions calculated and weighted for each layer, we can obtain the entire blurring distribution for subsurface reflection.

The calculation process illustrated in Fig. 6 shows the tracing of a ray away from the viewpoint, and sums up the reflection distributions differing in each layer from the surface to the deeper layer.

The extent of reflection distribution is controlled by the Beckmann function used in the Cook-Torrance reflection model. The Beckmann function is expressed by the equation given below.

$$D = \frac{\exp\left(-(\tan\delta / m^2)\right)}{m^2\cos^4\delta} \quad \cdots\cdots\cdots\cdots \quad (3)$$

Here, m is the parameter indicating the surface roughness, and δ is the angle between the surface normal and the micro-facet normal.

In the Cook-Torrance model, variable m has the physical meaning of the normal distribution of micro-facets, but in our model we handle this variable as a distribution parameter related with both the incident L_2 that reflects light in the V_2 direction and the micro-facet normal H.

It is usually taken for granted that the color of specular reflection is equivalent to the color of a light source. The pearl blurring component, however, is caused by the light that has entered the subsurface, and so we have allotted an object color according to the depth of the layer.

Compared with the Monte Carlo algorithm mentioned above, this algorithm is more approximate, but has the advantage that it requires the calculation of the only those rays that reach the eye, and that the amount of calculation can be scalable to the quality or calculation time required because the cost is proportional to the number of layers for which the reflection distribution is calculated. Figure 7 shows an example of the BRDF for an incident angle of 30° calculated by using this algorithm, with the graph showing sufficient approximation to the graph in Fig. 5.

This algorithm keeps the characteristic of the first algorithm, namely the direction becomes more and more deviated from the direct reflection as the ray moves deeper into the nacreous layer, while keeping the calculation cost comparatively low.

3.4 Image synthesis of blurring component

An example of the blurring component image synthesized by using the fast algorithm is given in Fig. 8, showing clearly the light source image at the center and the blurring around. The synthesized pearl image including this blurring component image is given in item 4.3 for the convenience of explanation.

4. Partial coherent interference model

In Section 2, the interference phenomenon independent of the direction of light source was taken into consideration to visualize the characteristic of the pearl interference phenomenon. However, even this model failed to describe fully the pearl interference phenomenon. In this section, therefore, we intend to take due account of the interference light dependent on the direction of the light source to propose a model based further on the real physical phenomena.

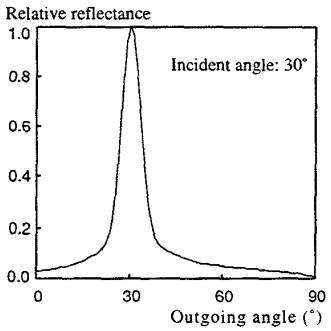

Fig. 7. An example of BRDF by fast simulation.

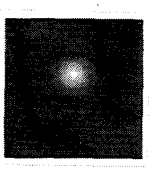

Fig. 8. An image showing blurring.

4.1 Failure in pearl representation using general thin-film interference model

Originally we carried out simulation on the assumption that the pearl interference phenomenon depended on the general thin-film interference model. During the process, however, the appearance of a strange image quite different from a real pearl made us abandon the general model and search for the new illuminant model mentioned in Section 2.

Here, we would like to confirm again the concept of a general thin-film interference. In a general thin-film interference, the hue distribution of the interference light greatly depends on the direction of light source apparently because of the dependency of the phase difference between two interference waves on the incident angle of the light. This phenomenon is seen in the shifting of the transmitted/reflected light spectrum of a narrow-band-pass filter or a multilayer thin film coating in the short-wave direction when the incident angle becomes larger. It can be easily observed that the light changes its color from green to blue, violet, red, etc. when a narrow-band-pass filter facing a light source is gradually inclined.

The synthesized images based on the conception of a general interference are given in Figs. 9a and 9b. The images looked fine at first. Figure 9a shows the image of interference component, and Fig. 9b the synthesized pearl image. However, when the light source position is changed, the interference component image and the synthesized image were changed as shown in Figs. 9c and 9d, and are quite different from the images of a real pearl.

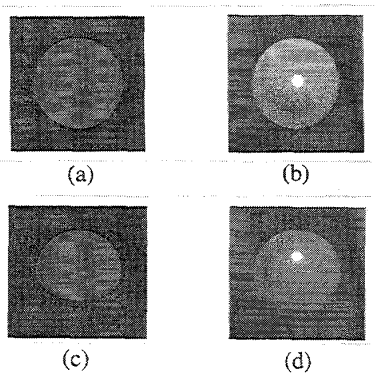

(a) Interference component image when the viewing direction is closer to the light source direction

(b) Synthesized image when the viewing direction is closer to the light source direction

(c) Interference component image when the viewing direction is away from the light source direction

(b) Synthesized image when the viewing direction is away from the light source direction

Fig. 9. Incorrect images based on a wrong model. (original: color)

After consideration it was revealed that no problem arose when the angle between the light source direction and the viewing direction was narrow, and that the incompatibility between the real and synthesized images appeared when the angle between the light source direction and the viewing direction became wider. Further observations and simulations showed that the interference hue was always distributed concentrically from the center of the sphere, which led us to develop a model which was independent of the direction of the light source.

4.2 Partial coherent interference model

We have succeeded in explaining the concentric distribution of the interference hue from the center of the sphere, and in synthesizing pearl-like images by using the illuminant model. It is true that the concentric distribution of the interference hue is the main feature of the pearl interference as mentioned in the previous subsection, but it does not necessarily mean that the pearl does not also have general thin-film interference.

Actually, interference light whose hue changes as the light source is moved is found inside the shell of a pearl oyster, the mother shell of pearl, with a flat nacreous layer like that of a pearl. This indicates that the general thin-film interference also occurs in the nacreous layer, and a careful observation of the pearl shows that the hi-light does get slightly colored, which contributes to the improvement in pearl-like quality, especially to the sense of brightness.

In other words, the interference phenomenon observed in a pearl is the mixture of the interference of hi-light (spatial coherent light), dependent on the direction of light source, and the interference of multiple reflection of light (spatial incoherent light), so that it is necessary to take account of both elements in order to carry out modeling of the interference seen in a pearl and to synthesize the pearl images.

We call this model the "partial coherent model", since both coherent and incoherent light are taken into account.

4.3 Image synthesis

Examples of synthesized images obtained through the partial coherent model and the blurring model mentioned in the above subsection are given in Fig. 10, with Fig. 10a showing an image of interference component of coherent light and Fig. 10b the mixed image of Fig. 10a and the interference component of incoherent light obtained through the illuminant model.

Figure 10c shows a synthesized pearl image containing both the partial coherent interference image in Fig. 10b and the blurring component image in Fig. 8. Both the concentric hue distribution of interference light and the coloring of hi-light are visualized with no sense of incompatibility, providing an additional feel of pearl-like quality, and slightly contributing to the improvement in the sense of brightness. Further, the contrast between hi-light and blurring gives a synergistic effect to further improve the sense of brightness, proving that blurring is an important factor in the visualization of a pearl.

5. Implementation to the simulator

A visual pearl-quality evaluation simulator was built using the visualization technique in order to synthesize the virtual pearl images. Figure 11 shows an example of the visual pearl simulator. Using this simulator, virtual sample images of various qualities can be synthesized by manipulating the parameters given below.

(1) Sense of depth (intensity of interference component and diffuse reflection component)
(2) Sense of brightness (directivity of the specular reflection and distribution of blurring)
(3) Sense of grain (texture strength)
(4) Object color (hue of diffuse reflection component)
(5) Interference color (hue of interference component)
(6) Direction of light source

We can visualize how the physical parameters contribute to the pearl quality by changing the values of the operating amount of these parameters.

The simulator is implemented on an SGI Power Onyx graphics workstation. It takes a few minutes to prepare an look-up table for the interference component, but once made, the interference component images can be synthesized only by using the look-up table. The time needed to synthesize the images of components other than the interference component is in the order of a few seconds for a 200 x 200 resolution image, which we think is within a permissible range of time.

Furthermore, this simulator is equipped with a superimposition function, and is capable of placing a synthesized image in a real scenes. Example of synthesized images in a real scenes are shown in Fig. 12.

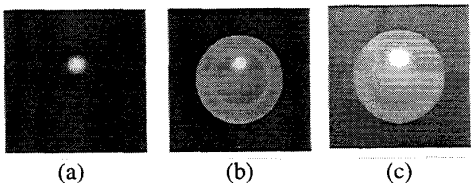

(a) (b) (c)

(a) Coherent light interference image
(b) Partial coherent interference image
(c) Synthesized image

Fig. 10. A synthesized image with inteference and blurring. (original: color)

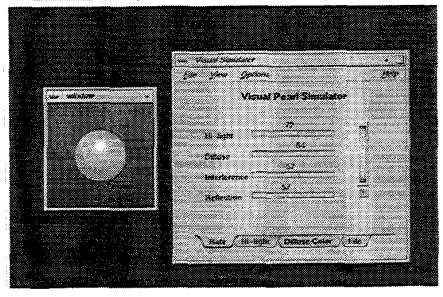

Fig. 11. A pearl visual simulator. (original: color)

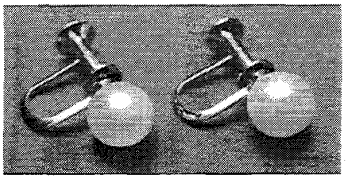

(a) Synthesized image (left) and real image (right)

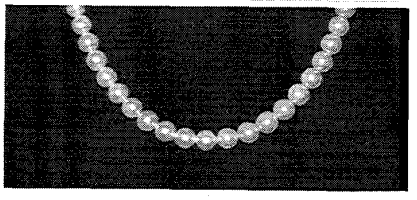

(b) Real image (left half) and synthesized image(right half)

Fig. 12. Superimposition of synthesized images on photos of real pearls. (original: color)

The superimposition of the synthesized pearl images and real scenes is useful not only for quality evaluation, but also for wide applications such as the designing jewelry and ordering through the Internet. With the time currently required for calculation and the present level of image quality, before long the simulator will be able to be applied to experience the feeling of a product in a catalog by placing synthesized jewelry on the facial image of customers at jewelry shops, or in a virtual jewelry design system allowing the interactive design of made-to-order jewelry.

6. Conclusion

We have proposed an image synthesis algorithm and physical models of interference and blurring for pearl visualization based on physics-based modeling. In order to represent the blurring caused by the subsurface reflection, two models, based on the Monte Carlo method and on the reflection distribution, were proposed and compared. Both models were found to provide sufficient quality for pearl representation, so we adopted the latter model which had lower calculation costs. As for the representation of pearl interference, we adopted the interference model for both coherent light and incoherent light to visualize the physical phenomena more exactly. We synthesized the pearl images to confirm the improvement in the sense of brightness and pearl-like quality.

Further, we implemented these functions on a simulator to carry out the real-time synthesis of virtual and real pearl images, and confirmed that this system could be put into practical use in the jewelry shops.

In the future, we plan to introduce natural fluctuations and irregularities to build a model much closer to the physical phenomena of a pearl. Further, we are determined to study information compression and speeding up the calculation by using the elementary factor of "pearl-like quality".

References

[1] S. Tokai, M. Miyagi, T. Yasuda, S. Yokoi and J. Toriwaki, "A Method for Rendering Citrus Fruits with Computer Graphics", Trans. IEICE, vol. J76-D-2, no. 8, pp. 1746-1754 ,1993 (in Japanese)

[2] E. Groller, R.T. Rau and W. Straber: "Modeling and Visualization of Knitwear", IEEE Trans. Visualization and Computer Graphics, 1, 4, 302-310, 1995

[3] N. Nagata, M. Kamei, M. Akane and H. Nakajima: "Development of a Pearl Quality Evaluation System Based on an Instrumentation of "Kansei"", Trans. IEE Japan, vol. 112-C, no. 2 ,1992 (in Japanese)

[4] N. Nagata, M. Kamei and T. Usami: "Factors Identification Using Sensitivity of Layered Neural Networks and Its Application to Pearl Color Evaluation", Trans. IEE Japan, vol. 116-C, no. 5, pp.556-562, 1996 (in Japanese)

[5] N. Nagata, T. Dobashi, Y. Manabe, T. Usami,S. Inokuchi: "Modeling and Visualization for a Pearl-Quality Evaluation Simulator", IEEE Trans. Visualization and Computer Graphics, Vol. 3, No. 3, October-December, 1997

[6] K. Wada, Pearl. The national jewelry association, 1982 (in Japanese)

[7] J.S. Gondek, G.W. Meyer and J.G. Newman: "Wavelength Dependent Reflectance Functions", Computer Graphics Proc., Ann. Conf. Series, 213-220, 1994

[8] P. Blasi, B.L. Saec and C. Schlick: "A Rendering Algorithm for Discrete Volume Density Objects", EUROGRAPHICS '93, 12, 3, C201-C-210, 1993

[9] T. Nishida, Y. Dobashi and E. Nakamae: "Display of Clouds Taking into Account Multiple Anisotoropic Scattering and Sky Light", Proc. SIGGRAPH '96, 1996-8, 379-386, 1995

[10]P. Hanrahan and W. Krueger: "Reflection from Layered Surfaces due to Subsurface Scattering", Computer Graphics Proc., Ann. Conf. Series,213-220, 1994